Tropical monsoons around Africa: Stability of El Niño–Southern Oscillation associations and links with continental climate

Mark R. Jury

Geography Department, University of Zululand, Zululand, South Africa

Dave B. Enfield

Atlantic Oceanography and Meteorology Lab, National Oceanic and Atmospheric Administration, Miami, Florida, USA

Jean-Luc Mélice

Centre IRD de Bretagne, Plouzané, France

[1]   Interannual fluctuations of monsoons around Africa and the stability of associations with the El Niño–Southern Oscillation (ENSO) and African rainfall are studied. The statistical analysis employs sea surface temperature (SST), surface and upper winds, and surface pressure averaged over key monsoon areas of the tropical Atlantic and Indian Oceans. The time series span the period 1958–1998, and wavelet analysis is applied to localize relationships in time as well as in frequency and enable us to examine how the amplitude and time delay at interannual scales varies through the record. Comparisons are made with Niño3 SST and other known ENSO signals in the African hemisphere. It is found that upper zonal winds over the tropical Atlantic are an integral part of the global ENSO. Zonal winds are associated with SST changes in the equatorial east Atlantic, which are antiphase to those in the west-central Indian Ocean. A composite analysis of warm and cool events in the Indian Ocean reveals that evaporation, radiative fluxes, and wind curl interact constructively. Anticyclonic curl (depression of isotherms) leads warm events, while cool events may initiate from oceanic advection and are sustained by evaporative fluxes. Rainfall fluctuations across Africa are analyzed, and three coherent areas are identified: West (Sahel-Guinea), Southern (Kalahari-Zambezi), and East (Kenya-Tanzania). Multivariate regression algorithms are fitted to the continuous filtered rainfall series over the period 1958–1988. Using three monsoon indices in a multivariate model, about 40% of the variance is explained at zero lag. An influential variable for most African rainfall areas is the zonal wind over the tropical Atlantic. The north-south SST gradient in the tropical Atlantic modulates rainfall in West Africa as expected. At 6 month lead, surface pressure in the north Indian Ocean is a key determinant for West African climate. For southern African rainfall, SST in the southwest Indian Ocean and monsoon indices in the west-central Indian Ocean play significant roles. East African rainfall fluctuations are linked with zonal winds in the east Indian Ocean. The findings address current Climate Variability and Predictability program (CLIVAR) priorities for understanding how continental climate interacts with ENSO and other regional modes of variability.   *INDEX TERMS:* 1620 Global Change: Climate dynamics (3309); 1635 Global Change: Oceans (4203); 3339 Meteorology and Atmospheric Dynamics: Ocean/atmosphere interactions (0312, 4504); 3354 Meteorology and Atmospheric Dynamics: Precipitation (1854); *KEYWORDS:* African climate, tropical Atlantic, Indian Ocean, monsoon

1.   Introduction

[2]   The tropical east Atlantic and west Indian Ocean exhibit seasonal monsoon circulations of varying extent and intensity, dependent on north-south contrasts in temperature induced by the landmasses of Africa and Asia. Interhemispheric flow from the south intensifies from May to September, bringing convective rains to the northern tropics, from India to the African Sahel. The weaker northeast monsoon flowing out of Asia in the months November to March, extends convective rains into the southern tropics from Madagascar to Angola. The depth and orientation of the shallow monsoon circulation and its embedded weather systems depend on the upstream character of ocean-atmosphere interactions. Surface heat fluxes result in cooling of the tropical oceans, leading to an increase in the north-south thermal gradient, a strengthened Hadley cell and an ampli-

fied seasonal cycle. Zonal circulation cells extending toward Africa interact with the monsoon circulations and remote El Niño–Southern Oscillation (ENSO) and contribute to interannual fluctuations of climate, our focus here. It is generally accepted that the Indian Ocean behaves differently than the Atlantic and Pacific. Equatorial upwelling is not well-defined, and the zonal slope of the thermocline is weak. Thus our analysis needs to account for these differences, while seeking to explain some of the monsoon-ENSO interactions around Africa.

[3] Africa experiences climatic extremes lasting from seasons to decades. Persistent dry and wet spells have a proportionately large influence on economic output because more than half of African GDP is derived from subsistence agriculture [*Rwelamira and Kleynhans*, 1996]. Runoff averages 16% of rainfall across the continent of Africa [*Peixoto*, 1993] and river flows have exhibited declining trends in the past 50 years (M. R. Jury, Composite climate structure modulating the interannual variability of African river flows, submitted to *Journal of Hydrology*, 2001, hereinafter referred to as Jury, submitted manuscript, 2001). Rainfall over the western Sahel has shown a steady decline in recent decades in association with significant multidecadal to centennial variability. These trends and variations together with rain-dependent economic structures make the continent particularly vulnerable to cycles of drought and flood. Many authors have studied the extent, patterns and temporal nature of rainfall fluctuations in Africa [*Nicholson*, 1986; *Janowiak*, 1988] and have identified three coherent regions: Sahelian belt of West Africa, subtropical southern Africa, and equatorial east Africa. Each has a unique seasonal character and different assimilation of remote teleconnections from surrounding monsoons resident over the tropical east Atlantic and west Indian Oceans. The Sahel rainy season is from June to September, during which time easterly waves travel along defined latitude bands, fed by the Guinea monsoon [*Long et al.*, 1998]. East Africa experiences bimodal rains peaking in November and April associated with passage of the ITCZ and attendant Hadley circulations. Interannual rainfall variability is often attributed to zonal circulations of the Indian Ocean [*Hastenrath et al.*, 1993; *Hastenrath*, 2001; *Mpeta and Jury*, 2001], particularly with regard to an east-west dipole in climatic anomalies [*Webster et al.*, 1999]. Over southern Africa rains occur from November to March in the form of meridional bands – positioned according to standing subtropical waves and their response to tropical heat sources [*Harrison*, 1986]. A common factor throughout Africa is the intensity and length of the intervening dry season. Rainfall is absent up to 7 months of the year and springtime temperatures >40°C are common.

[4] Here, we explore climate variability in the African hemisphere guided by well known determinants: the El Niño–Southern Oscillation, a north-south gradient of SST in the tropical Atlantic [*Servain et al.*, 1998] and an east-west gradient of SST in the Indian Ocean [*Saji et al.*, 2001]. Pacific El Niño conditions are associated with warming of the west-central Indian Ocean [*Cadet*, 1985; *Latif and Barnett*, 1995; *Nicholson*, 1997; *Reason et al.*, 2000] and increased upper level westerly winds over Africa [*Harrison*, 1986; *Jury et al.*, 1999]. Such conditions induce drought across much of the continent [*Nicholson*, 1986; *Jury et al.*,

1994; *Rocha and Simmonds*, 1997], except for the eastern tropics [*Mutai et al.*, 1998; *Goddard and Graham*, 1999]. To further investigate ENSO influence in the Indian Ocean, a composite analysis of air-sea interactions is performed.

[5] The global ENSO often elicits a lagged or opposing response in the tropical Atlantic [*Hirst and Hastenrath*, 1983; *Nicholson and Nyenzi*, 1990; *Zebiak*, 1993; *Nicholson*, 1997]. Prior to the development of El Niño conditions in the eastern Pacific, the tropical eastern Atlantic Ocean begins to cool. A zonal overturning (direct) circulation arises [*Hastenrath*, 2001] with upper westerly/lower easterly flow linking subsidence over central Africa with uplift over central South America. Such a pattern contributes to a near-simultaneous decrease of most river flows across Africa (e.g., Nile, Niger, Zambezi, etc) except around Lake Victoria (Jury, submitted manuscript, 2001), through a sustained interaction between the convective systems and regional circulations [*Druyan and Hall*, 1996; *Ward et al.*, 1999]. In this manner the tropical Atlantic plays an important role in the transmission of ENSO throughout the African region.

[6] In this paper we investigate the temporal stability of monsoon indices and ENSO associations around Africa, through statistical analysis of observed data for key areas over the period 1958–1998. The nature of ocean-atmosphere coupling is assessed with a focus on the circulation over the equatorial Atlantic and air-sea interactions of the Indian Ocean. Varying contributions are evaluated for the surface heat fluxes, radiative balance and wind-forced ocean uplift in the development of warm and cold events. We then relate the monsoon indices to time series of continental rainfall via multivariate regression.

2. Data and Methods

[7] Monthly rainfall data across Africa for the period 1958–1988 is available from the French National Centre for Scientific Research [*Richard*, 1994; *Camberlin*, 1995]. Uneven station densities can influence statistical analyses, so some stations were excluded in high-density areas to create a more uniform spatial coverage. 466 stations having complete records were retained as shown in Figure 1. There are some gaps in coverage over Angola, etc that limit subsequent analysis in those regions. A Varimax rotated principal component (rPC) analysis was carried out on deseasoned departures of monthly rainfall [*Bigot et al.*, 1995]. The first 7 rPCs explained over half of variance. Here we make use of three modes, the 'west' African region comprising Sahel and Guinea areas (21% of variance), the 'southern' African region comprising Zambezi and Kalahari areas (15.5%), and the 'east' African region extending over Kenya, Tanzania and Lake Victoria (explaining 7% of variance). The rainfall time series, based on the rPC scores, are shown in Figure 2 and spatial loading patterns are schematically represented in Figure 3.

[8] We investigate relationships between the environmental variables and regional rainfall indices at 0 and 6 month lag using multiple regression models, with predictors inserted in a forward stepwise manner as outlined by *Jury et al.* [1999]. The rainfall time series are decomposed into seasons to study the influence of key predictors. Our purpose in regressing rainfall onto the environmental indi-
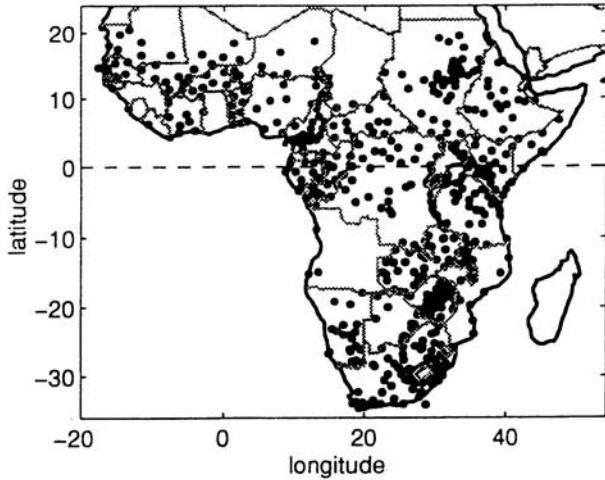
Figure 1. African rainfall stations used in the statistical analysis.

ces is to assess the interaction of ocean monsoons and terrestrial climate. All variables are wavelet-filtered to remove 6 and 12 month cycles, normalized by their standard deviation and smoothed with a 3 month running mean to reduce noise due to observational bias and intraseasonal fluctuations.

[9] In assessing the significance of statistical fit, we estimate the degrees of freedom (DF) as the sample size minus the number of predictors (three) divided by a measure of persistence [*Quenouille*, 1952]. The autocorrelation function declines below the 95% significance level in the case of West African rainfall at 10 months and in southern and east Africa at 7 months. With a total sample of 372 months, the DF for the persistent West African rainfall series is ∼37. The persistence is attributable to slower variations of SST in the tropical Atlantic [*Enfield et al.*, 1999]. For southern and east Africa the DF is ∼53.

[10] The selection of monsoon indices to describe the large-scale environment around Africa reflects an extensive body of research [e.g., *Rocha and Simmonds*, 1997; *Enfield and Mayer*, 1997; *Jury et al.*, 1999; *Reason et al.*, 2000]. They include key areas in the tropical Atlantic and Indian Oceans and correspond geographically to zonal circulation systems, regional monsoon flows, known SST responses to ENSO, and internal Atlantic (non-ENSO) variability. Tropical wind indices which anticipate changes in basin-scale SST are found in the east Indian [*Rocha and Simmonds*, 1997] and central Atlantic Oceans [*Zebiak*, 1993]. SST data for key areas were extracted from the Reynolds 2° × 2° reconstructed SST data set [*Reynolds and Smith*, 1994], while other atmospheric variables were extracted from the 1958–1998 NCEP/NCAR reanalysis climate data assimilation system (CDAS) archives [*Kalnay et al.*, 1996]. The monsoon indices are defined in Table 1 and are used in both the cross-wavelet analysis (section 3.1) and the regression analysis (section 3.3).

[11] Variables 1 and 5 describe monsoon circulations either side of Africa. The zonal wind components are part of the zonal direct circulation that include the ocean-driving low-level easterlies at the surface, while the meridional wind reflects the interhemispheric monsoon flow. Variables 1, 8

and 9 are indices known to vary with ENSO phase [*Jury et al.*, 1994, 1999]. Variables 5 and 6 describe the Indian Ocean response to ENSO [*Jury and Pathack*, 1993]. Variable 7 is known to modulate southern African climate [*Reason and Mulenga*, 1999]. Variable 2 represents the meridional SST gradient across the Atlantic [*Enfield et al.*, 1999], which is known to influence West African climate [*Servain*, 1991]. A total of 13 variables are considered in 10 key areas. The Niño3 SST (10) is utilized as a reference for ENSO teleconnections from the Pacific sector.

[12] We investigate interactions between environmental variables in the time-frequency domain, with the continuous
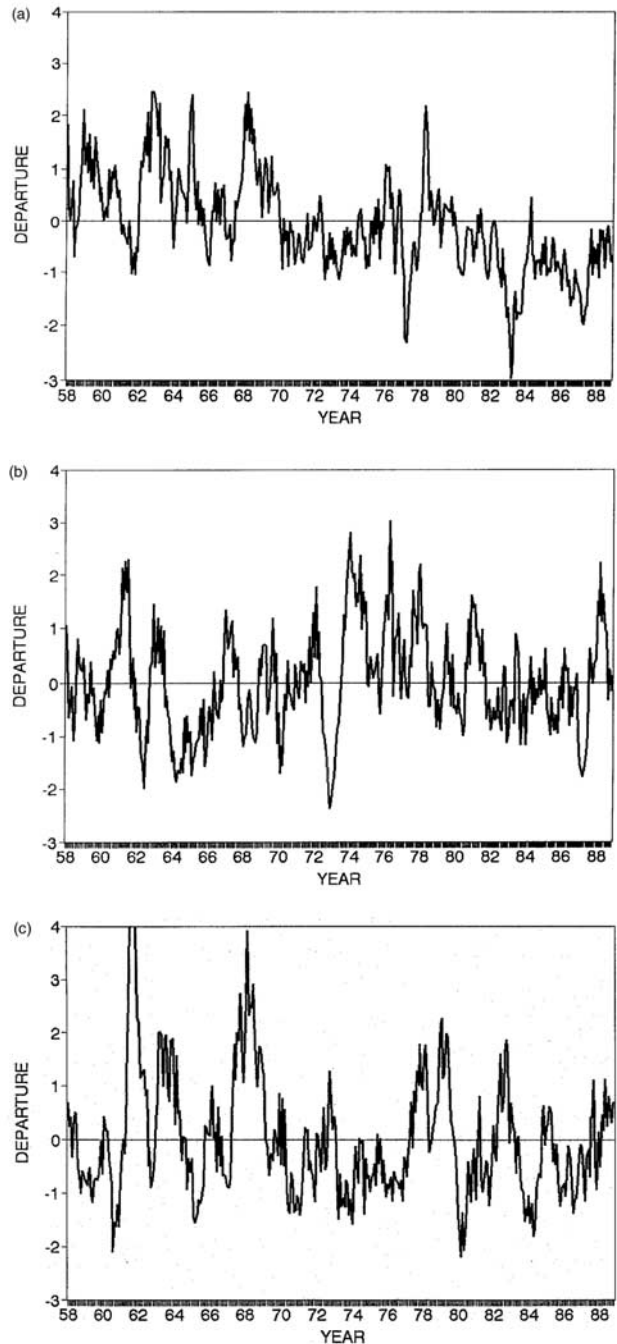
Figure 2. Rotated principal component time scores for (a) West Africa, (b) southern Africa, and (c) east Africa.
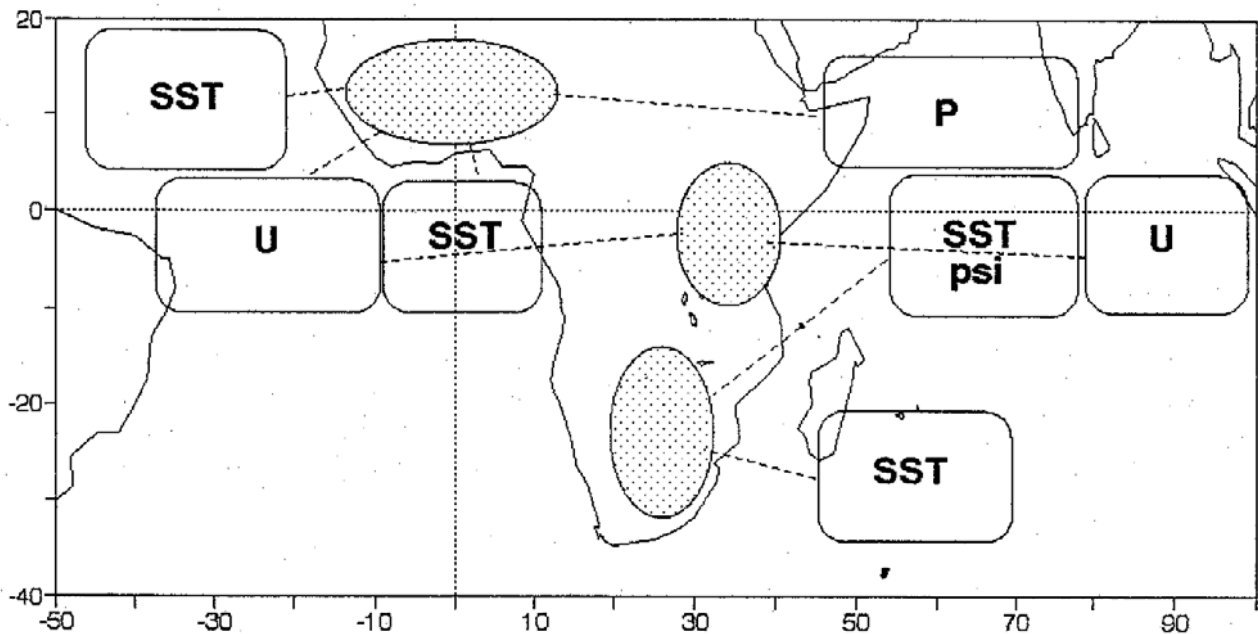
Figure 3. Schematic representation of spatial loading regions for African rainfall (shaded areas). The corresponding time scores appear in Figure 2. Rectangles identify tropical Atlantic and Indian monsoon index areas described in Table 1.

wavelet transform (CWT) technique [*Lau and Weng*, 1995; *Torrence and Compo*, 1997; *Mallat*, 1998]. The CWT is first applied to filter out the seasonal cycle embedded in the data. We then explore relationships within the environmental variables and terrestrial rainfall using the cross-wavelet spectrum. Meyers et al. (1993) has applied this type of analysis to evaluate ocean and atmospheric wave propagation. From this technique, we develop a method that allows estimation of the cross-wavelet amplitude and phase (or time delay) between the signals, localized in time. Its mathematical framework is given in Appendix A. There are edge effects in this type of analysis dependent on the spectral character of the signal. Here, the time delay is ambiguous for the first and last 3–4 years of the record (1958–1962 and 1995–1998), while elsewhere the delay may be unreliable when the cross-wavelet amplitude is small. The strongest justification for using wavelet methods is that they localize relationships in time as well as frequency and enable us to examine how the amplitude and time delay at interannual frequencies varies through the record. Correlation analysis, spectral analysis and other record length methods cannot do this. For example, correlation analysis can show a single-correlation value to characterize the relationship between two variables, with no indication of whether that reflects recurrent associations throughout the record or only a few strong events in part of the record; or whether it reflects primarily high or low frequencies, or even an unresolved trend.

[13] An additional problem is the nonstationary density of observations feeding the NCEP climate data assimilation system, which is likely to be worse in the early part of the records. Conventional observations over the oceans around Africa reach acceptable levels after the mid-1960s. In recent decades satellite observations supplement and improve our knowledge of SST and atmospheric circulation fields.

[14] With consecutive monthly data, it is necessary to remove the seasonal cycle while maintaining residual signals. This is accomplished via the CWT ridge procedure described by *Delprat et al.* [1992]. We illustrate in Figure 4 how the seasonal cycle is removed from the original central Atlantic upper zonal wind signal (Figure 4a). The CWT modulus (amplitude) of the wind signal is displayed in Figure 4b. The seasonal cycle in the CWT image consists of two ridges with periods close to 6 and 12 months. The difference between the original signal and the seasonal cycle (not shown) gives the filtered signal (Figure 4a, bold line). The CWT modulus of the filtered signal is displayed in Figure 4c. Note that the filtering process successfully removes the seasonal cycle and retains the interannual residual of interest.

[15] A brief analysis of subsurface thermal structure in the tropical Atlantic and Indian Oceans is conducted using data assimilated by the ocean model of J. Carton (Univ. Maryland-Delaware) available on the International Research Institute for Climate Prediction's Lamont Doherty Earth Observatory (IRI-LDEO) website. The model is an assim-

Table 1. Variables Used in the Analysis[a]

Variable	Area/Domain Averaged
U wind (cAu, cAu$_2$)	central Atlantic (5°N–10°S, 40°W–0°)
SST (nAst, seAst)	tropical north and southeast Atlantic (7°–23°N, 18°–42°W; 3°N–13°S, 13°W–11°E)
Pressure (nwIp)	northwest Indian Ocean (5°–15°N, 50°–80°E)
U,V wind (wIu,wIv)	west Indian Ocean (5°N–10°S, 40°–60°E)
SST, flux (cIst, cIe)	central Indian Ocean (15°N–15°S, 50°–80°E)
Stream function (cIΨ)	central Indian Ocean (10°N–10°S, 60°–85°E)
SST (swIst)	southwest Indian Ocean (20°–35°S, 45°–65°E)
Pressure (eIp)	east Indian Ocean (10°N–15°S, 80°–95°E)
U wind (eIu)	east Indian Ocean (3°N–10°S, 80°–100°E)
SST (Niño3)	Niño3 Pacific Ocean (5°N–5°S, 150°–90°W)

[a] All variables at surface, except for subscript 2 = 200 hPa ~12 km.
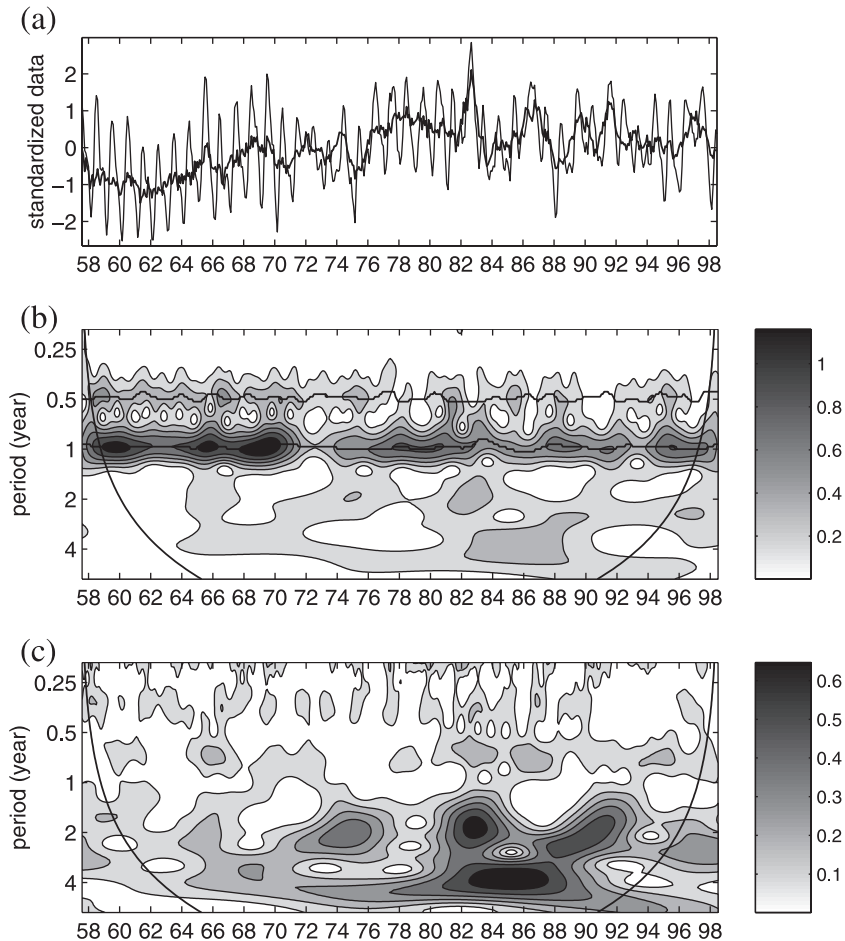
Figure 4. CWT analysis for the Atlantic upper zonal wind index: (a) the raw and CWT-filtered (bold) times series, (b) the CWT modulus of the raw series with continuous ridge lines, and (c) the CWT modulus of the filtered wind index. The CWT filter successfully cleans up the varying seasonal cycle.

ilation of available subsurface T and S observations, and surface wind fields (and calculated fluxes) on a $1° \times 1°$ global grid, monthly in the period 1950 to 1998. The model horizontal resolution is $2°$ longitude by $1°-2°$ latitude (more dense near the equator). The vertical resolution is 20 m near the surface and decreases with depth. The departure in the depth of the $20°$ isotherm from the long-term mean (dZ_{20}/dx anomaly) is evaluated on the equator at $0°$ and $30°$W, and at $60°$ and $90°$E for various seasons. The analysis is carried out for composite ENSO years using two criteria: Niño3 SST and southern African rainfall in accordance with M. R. Jury and S. J. Mason (Evolution of ENSO teleconnections around southern Africa, Water SA, submitted, 2001). We assess the extent to which the thermocline in both oceans heaves westward during Pacific El Niño conditions, when dry weather is experienced across much of Africa.

[16] In our tropical Atlantic analysis, key variables are combined into an index for comparison with Atlantic hurricane activity, based on information supplied by C. W. Landsea (personal communication, 2000). A three-way index is calculated from standardized departures by subtracting the 200 hPa zonal winds in the central Atlantic from the surface winds, and adding the tropical north Atlantic SST. This index increases as SST increases and tropospheric wind shear decreases, both of which favor greater hurricane development in the tropical North Atlantic [*Gray*, 1984; *Goldenberg and Shapiro*, 1996; *Landsea et al.*, 1999]. The hurricane activity index is the number of storm days with winds >33 m s^{-1} in the Atlantic basin $10°-40°$N, $40°-100°$W.

[17] In our study of the tropical west Indian Ocean the heat budget is assessed using variables 5 and 6 from Table 1, together with the estimated shortwave (Qs) and longwave radiation (Ql) and the sensible heat flux (Qh). All data are extracted from NCEP reanalysis archives in the area $10°$N–$15°$S, $50°-80°$E.

3. Results
3.1. Temporal Stability of Monsoon-Enso Relationships 1958–1998

[18] In this section, we analyze the statistical association between key environmental variables over the 41 year study period. We first explore the relationship between the Niño3 SST and the central Atlantic upper zonal winds (Figure 5a) with the cross-wavelet spectrum technique (see Appendix A). The modulus (amplitude) of the cross-wavelet spectrum of the two signals is displayed in Figure 5b. In analogy with a Fourier spectrum, the modulus corresponds to the cross-spectral energy, except that it varies with frequency and time. The region under the bold line in Figure 5b indicates
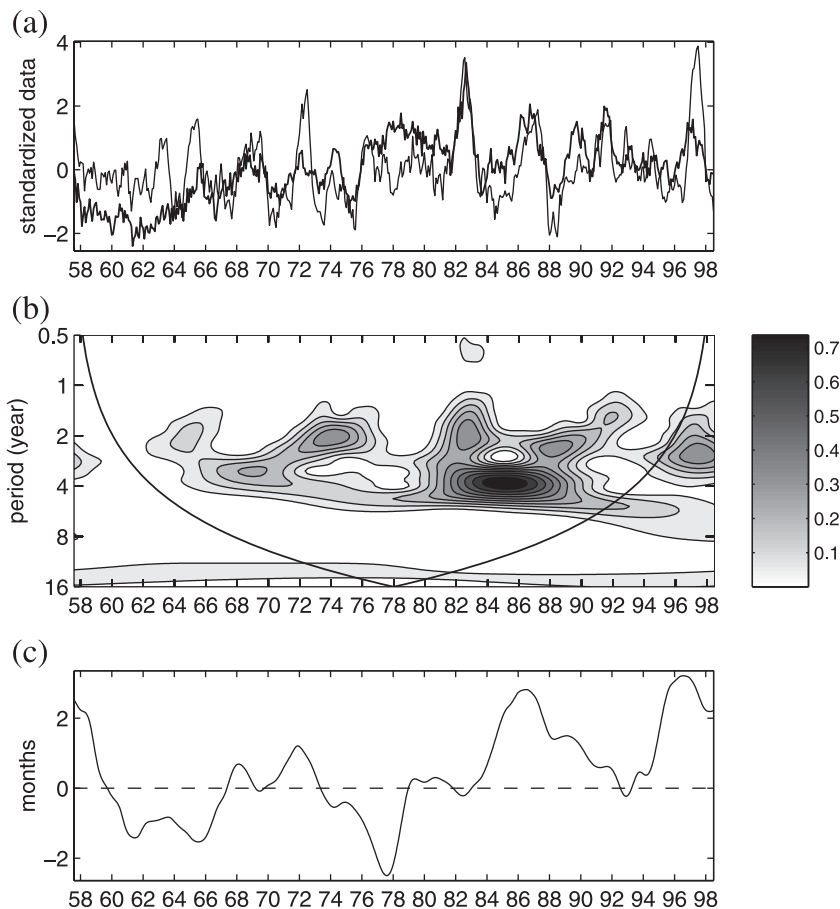
Figure 5.　(a) Filtered time series for Niño3 SST and upper zonal winds (bold) of the central Atlantic, (b) cross-spectrum modulus, and (c) instantaneous time lag, positive when the winds lead.

the area where edge effects are important, and results should be disregarded there. Largest amplitudes are concentrated in the 1.5–5 year interval. The relationship between the signals is temporally variant, e.g., fading in and out. Surges in the cross-wavelet modulus can be clearly seen centered on ENSO-related features: the El Niño events of 1969–1970, 1972–1973, 1982–1983, 1987, and 1997–1998, and the La Niña events of 1974–1976, 1989, and 1996. The time series in Figure 5a indicates a close coupling between Pacific ENSO and zonal circulation anomalies over the Atlantic. The 200 mb anomalies modulate the climatological mean Atlantic Walker cell, which is comprised of easterlies near the surface and westerly flow aloft that connects upper level outflow over the Amazon convective region with convergence aloft over West Africa. Some of this variability may be associated with the eastward propagating ENSO wave outlined by *White and Cayan* [2000].

[19]　We further investigate this relationship by calculating the time-varying instantaneous lag between the time series in the range 1–8 years, using the procedure described in Appendix A. Because of the wavelet filter imposed on continuous anomaly data, the results are independent of season. The instantaneous time lag between the Atlantic upper zonal wind and the Niño3 SST is displayed in Figure 5c. Its mean value is near zero. However, we observe that when the cross-wavelet spectral amplitude is large, the Atlantic upper wind leads Niño3 SST by 1–2 months. The

correlation between the wind and SST signals, continuously shifted in time by the instantaneous lag is 0.542, while the maximum correlation between the signals using the conventional approach is 0.461 at a lag of 1 month (winds leading). The higher correlation for the fluctuating lag between signals demonstrates the advantage of this approach. Why should the upper zonal flow over the equatorial Atlantic precede the Pacific Niño3 SST index? We believe it is because the tropospheric direct circulation (anomalous zonal overturning) reacts more quickly to eastward shifted convection in the Pacific than do east Pacific SSTs, which depend on the comparatively slow eastward propagation of ocean anomalies. The comparatively short timescale of the upper tropospheric response to a large scale diabatic heating anomaly near the dateline is related to the expected (atmospheric) Kelvin wave propagation eastward of the forcing [*Gill*, 1980]. In other words, both the Niño3 and the Atlantic winds are responding to atmospheric convective forcing in the western Pacific, but Niño3 responds slowly (oceanic response) and the Atlantic winds quickly (through the tropospheric Walker Circulation).

[20]　The upper tropospheric zonal wind anomaly is easterly (westerly) prior to (after) the late 1970s. This is consistent with a strengthening of the zonal direct circulation over the equatorial Atlantic during the DJF season, and is associated with a large scale climate shift that occurred around 1978 [*Mestas-Nuñez and Enfield*, 2001]. The accel-
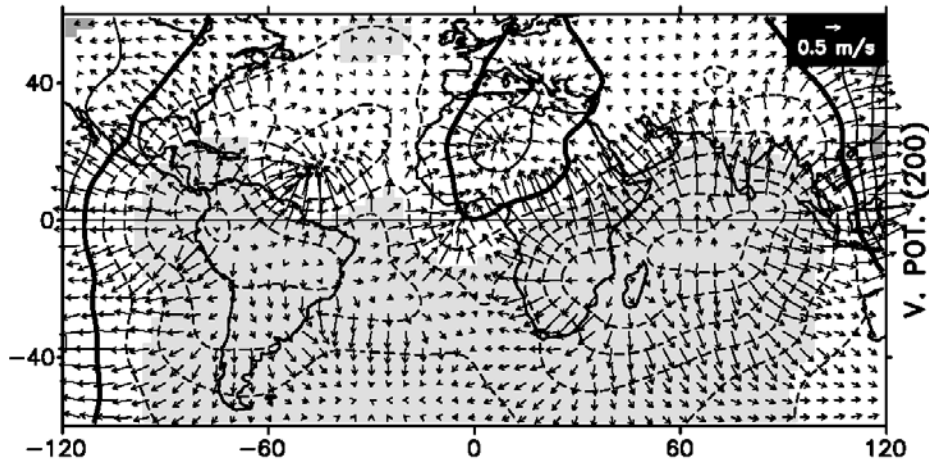
Figure 6. The change in the tropospheric circulation for DJF season before and after 1978, calculated by subtracting the 200 hPa composite mean velocity potential (contours) and irrotational velocity (vectors) for 1949–1977 from that of 1978–1999.

erated 200 hPa flow is part of a pattern that links greater Amazon convection and 200 hPa outflow over northern South America with increased subsidence and inflow over West Africa and the Gulf of Guinea (Figure 6). A con-

spicuous feature is an increase of outflow over the west-central Indian Ocean.

[21] Relationships between upper and surface zonal winds over the central Atlantic are considered in Figure 7.
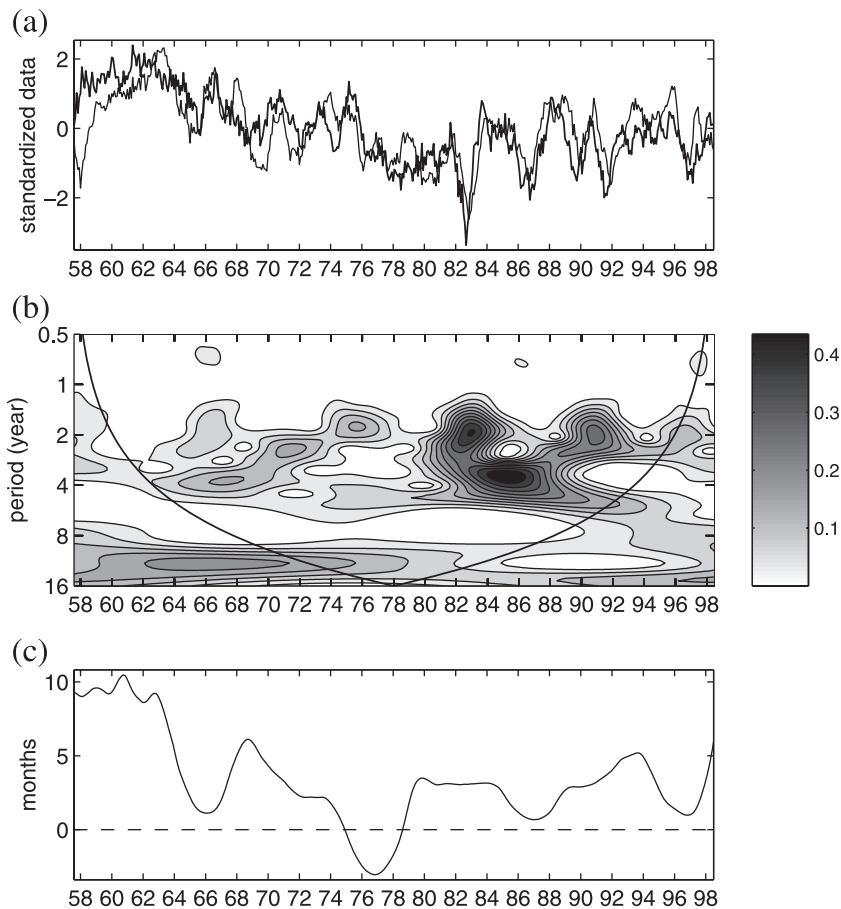
Figure 7. (a) Filtered time series for surface and upper (bold inverted) zonal winds of the central Atlantic, (b) cross-spectrum modulus, and (c) instantaneous time lag, positive when upper winds lead.
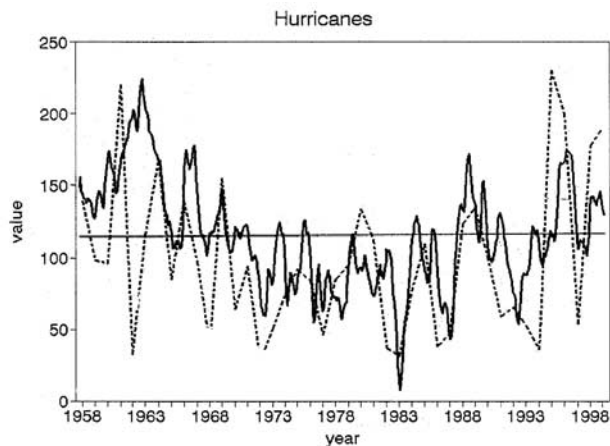
Figure 8. Filtered continuous time series of our three-way index ($cAu − cAu_2 + nAsst$), and July October Atlantic hurricane activity (dashed), based on storm day information provided by Landsea (personal communication, 2000).

The cross-wavelet modulus is displayed in Figure 7b and the instantaneous lag (mean = 3.4 months) between the upper and surface winds is plotted in Figure 7c. When calculated with a fluctuating lag, the correlation coefficient between the signals is −0.82. The conventional lagged correlation is −0.72 at 2 months (upper winds leading). The instantaneous lag shows small but probably insignificant fluctuations about this value, while the large lags at the beginning of the record are unreliable due to edge effects and because the cross wavelet modulus is small. In the earlier part of the record sustained lower (upper) westerly (easterly) anomalies are associated with greater rainfall over West Africa. The subsequent decrease in West African rainfall, and the Sahel drought, are consistent with the acceleration of the direct circulation as shown in Figure 6 [*Mestas-Nuñez and Enfield*, 2001]. More regular interannual fluctuations are seen after 1980 when Africa experienced drier conditions. The stable antiphase association suggests a prominent zonal direct circulation in agreement with *Hastenrath* [2001]. *Janicot et al.* [1998] described and simulated the interannual coupling between the zonal direct circulation in the Atlantic and equatorial SST in the Pacific.

[22] The African-Atlantic climate relationships include an association with the frequency of major hurricane development near 10°N, south and west of the Cape Verde Islands. *Gray* [1984], *Goldenberg and Shapiro* [1996], and *Landsea et al.* [1999] describe how ENSO phase modulates Atlantic hurricane activity in this region through local SST and vertical shear anomalies. Although located south of the hurricane development region, our equatorial Atlantic vertical wind shear anomalies (200 hPa minus surface winds) appear associated with the development process at both the interdecadal and interannual timescales. The three-way index (sum of normalized vertical shear and tropical North Atlantic SST) closely tracks western Atlantic hurricane activity as shown in Figure 8. At the interdecadal timescale, the peak in the early 1960s is followed by a long trend of declining tropical cyclone days culminating in the 1983 El Niño event. Thereafter a

gradual recovery occurs with upper easterly winds, lower westerly winds and a warmer north tropical Atlantic enhancing hurricane activity [*Goldenberg et al.*, 2001]. At the interannual timescale we also see strong in-phase agreement, although this breaks down briefly in the early 1960s and early 1990s. These features are consistent with the findings of past hurricane studies and suggest that our three-way index captures key aspects of the large scale environment (wind shear and SST) affecting the development of Atlantic hurricanes; e.g. increased upper easterlies/lower westerlies with respect to La Niña conditions, occur on the equatorward flank of the hurricane development axis and impart cyclonic vorticity.

[23] The Niño3 association with equatorial SST differences on either side of Africa (e.g., west-central Indian Ocean minus east Atlantic) is illustrated in Figure 9. The cross-wavelet modulus is displayed in Figure 9b and the instantaneous lag (mean = −1.5 months) is plotted in Figure 9c. The lag is computed for the 1–8 year range as before. The instantaneous lag correlation is 0.67, while the conventional correlation is 0.55 at 2 month lag (Pacific leading). The coupling shown by the cross-wavelet modulus is relatively stable with the Pacific ENSO being contemporaneous with Indian-Atlantic SST over most of the period except for 1961–1970 when Niño3 leads. The same ENSO-related features discussed for Figure 5b are also seen in Figure 9b. During El Niño years, when the east Atlantic SST is cool and west-central Indian Ocean is warm, rainfall decreases over much of Africa [*Jury*, 2001]. Hence, this relationship is opposite to that of Atlantic minus Pacific SST differences with respect to Caribbean and Central American climates [*Enfield and Alfaro*, 1999; *Giannini et al.*, 2000], which are wetter when the North Atlantic is warm and the eastern Pacific is cool. The antiphase relationship between the southeast Atlantic and west-central Indian Ocean SST is significant during the period 1969–1990 (coincident with strong ENSO oscillations), and is more quiescent in the early 1990s and early 1960s when ENSO activity was also weak. Where it exists, the relationship suggests that cool tongue conditions in the equatorial Atlantic precede west-central Indian Ocean warming (r = 0.33 at 9 months). Our results therefore suggest that the equatorial thermocline heaves toward the west in both oceans during ENSO phase transitions in a manner consistent with the SST changes.

[24] To test this concept, composite dZ_{20}/dx anomalies are analyzed from the Carton ocean data assimilation model. Atlantic thermocline slope anomalies (0°–30°W) prior to El Niño cases (Africa – mostly dry) are upward to the east at +1.7 10^{-6}, yielding an increase in the normal eastward upslope, and thus are consistent with a cooler eastern Atlantic. Prior to La Niña cases (where most of Africa is wet) the slope anomalies are downward to the east at −1.6 10^{-6} (warmer eastern Atlantic). Composite Z_{20} slope anomalies in the Indian Ocean (60°–90°E) during dry El Niño cases are upward to the east at +5.9 10^{-6}, and during wet La Niña cases slope anomalies are downward to the east at −5.1 10^{-6}. The subsurface thermal structure is consistent with the antiphase expression of SSTa either side of Africa, as expected. The Atlantic leads the Pacific, while the Indian Ocean follows. The amplitude of dZ_{20}/dx variability is three times higher in the Indian Ocean in January than in the
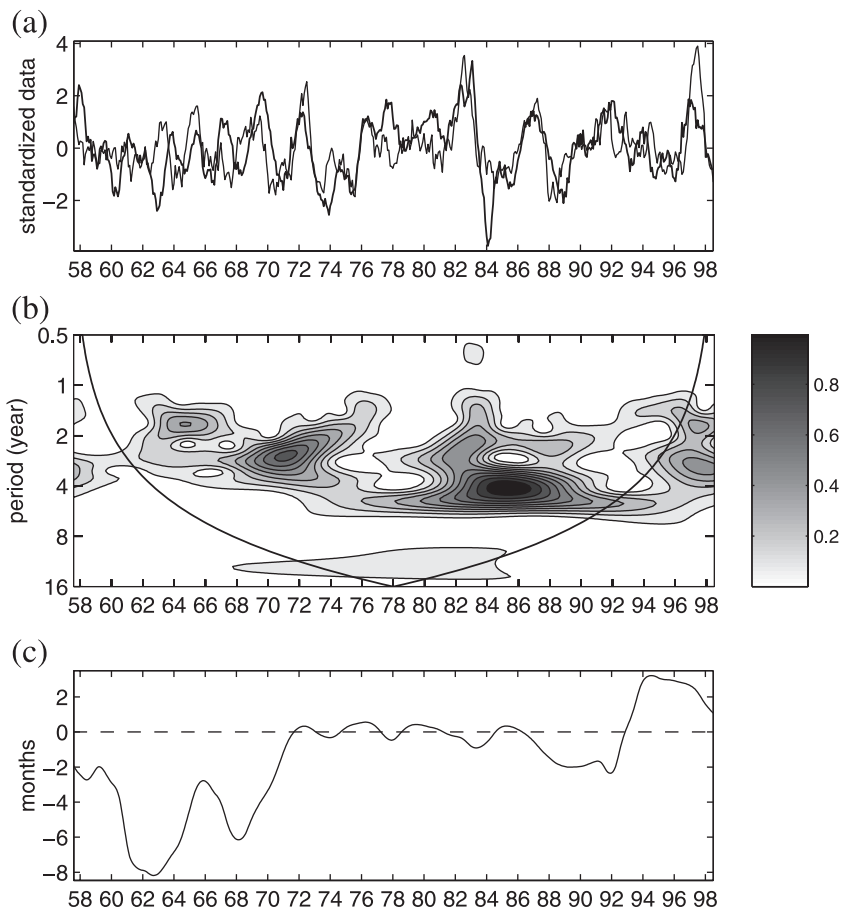
Figure 9. (a) Filtered time series for the SST difference between the west-central Indian Ocean and the east Atlantic (bold) and Niño3 SST, (b) cross-spectrum modulus, and (c) instantaneous time lag, positive when the SST difference leads.

Atlantic Ocean in the preceding July. For the west equatorial Indian Ocean, the Z_{20} depth averages 95 m during cool events and 115 m in warm events. For the east equatorial Atlantic the Z_{20} depth is 35 m before La Niña and 25 m before El Niño events. The concept that the thermocline heaves westward during onset and mature phases of El Niño is supported.

[25] The relationship between west-central Indian Ocean SST and surface winds over the east Indian Ocean is investigated in Figure 10. The instantaneous lag correlation is −0.66 and the mean delay is −2.2 months (winds leading). A significant portion of the variability is related to Pacific Niño3 SST. Hence, easterly wind anomalies occur in the eastern Indian Ocean, increasing upwelling west of Sumatra and an increase in the zonal slope of the thermocline at the onset of El Niño. SSTs rise to the west as the thermocline deepens there. This is consistent with equatorial ocean dynamics: a westward wind stress anomaly over the equator must be balanced by an eastward pressure gradient anomaly (increased thermocline slope). This ENSO-modulated east-west dipole is consistent with the findings of *Webster et al.* [1999], *Hastenrath* [2000], and B. Huang, and J. L. Kinter (The interannual variability in the tropical Indian Ocean and its relation to El Niño−Southern Oscillation, submitted to *Journal of Geophysical Research*, 2001, hereinafter referred to as Huang and Kinter, submitted

manuscript, 2001), who study its evolution using extended EOF analysis applied to heat content anomalies.

3.2. Atmospheric Forcing of Composite Events in the West-Central Indian Ocean

[26] The above analysis, as also that of *Reason et al.* [2000], confirms that much of the ENSO influence on the monsoonal processes relevant to African rainfall is mediated by Indian Ocean SST. Hence, we are interested to inquire as to how warm and cool years in the Indian Ocean are forced. A number of numerical models of the Indian Ocean, and global general circulation models, have successfully simulated the seasonal circulation of the Indian Ocean [*Woodberry et al.*, 1989; *McCreary et al.*, 1993; *Schiller et al.*, 2000]. Other research indicates that much of the variability is related to Pacific ENSO fluctuations [e.g., *Chambers et al.*, 1999]. However, SST variability has been less successfully simulated because of its greater dependence on sea surface fluxes that are poorly estimated [*Schiller*, 1999]. *McCreary et al.* [1993] showed that advection is important for SST in the boundary regions where upwelling cyclically produces large horizontal gradients of mixed layer temperature, but that elsewhere a layered model that includes a realistic mixed layer will fail to simulate mixed layer temperature when parameters needed for surface fluxes are suppressed. Their work suggests that over a large
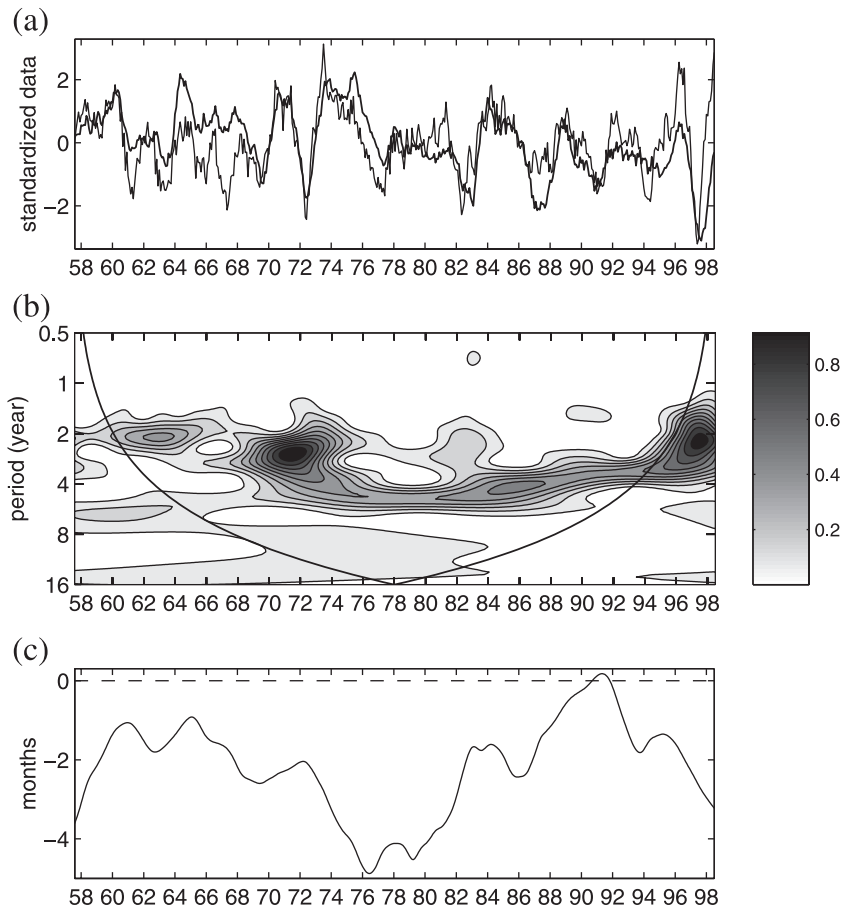
Figure 10. (a) Filtered time series of SST in the west-central Indian Ocean (inverted in bold) and surface zonal winds in the east Indian Ocean, (b) cross-spectrum modulus and (c) instantaneous time lag, positive when SST leads.

interior region where SST anomalies can mediate monsoon effects, the mixed layer heat budget may be dominated by a balance between surface fluxes and entrainment across the mixed layer base. It is with this in mind that we now explore the possible role of such a balance over a large interior region of the west-central Indian Ocean straddling the equator (Figure 3).

[27] ENSO-monsoon interactions over the west-central Indian Ocean cover a wide area $\sim 10^{13}$ m^2 and significantly affect the climate of surrounding countries (M. R. Jury et al., Motivations for an Indian Ocean observing system and applications to climate impacts and resource predictions in surrounding countries, submitted to *Journal of Geophysical Research,* 2001). Composite events in the Indian Ocean (10°N–15°S, 50°–80°E), are analyzed in Figures 11 and 12 through estimation of the heat budget imparted by surface fluxes and vertical motion induced by winds. We identify a group of warm cases (1970, 1993, 1983, 1987, 1992, 1998) and cool cases (1965, 1972, 1974, 1976, 2989, 1997) based on the SST anomaly (variable 5 in Table 1) exceeding 1 sigma with a peak in austral summer (DJF). The predicted SSTa (T_0 + dT) based on the net heat flux anomalies and flux plus entrainment anomalies is compared with the observed SSTa over the west-central Indian Ocean. In this analysis ocean-atmosphere interactions are assumed to be uniform over the domain.

[28] Ocean-atmosphere coupling is explored based on the assumption that cooler SST will derive from increased evaporation (Qe), entrainment cooling from below through isotherm uplift (cyclonic wind stress curl), and reduced shortwave radiation. While variables derived from the wind fields (e.g., flux and entrainment) are interpolated from observed data, radiative anomalies are derived in the NCEP model and vary according to estimated cloud cover. To calculate the change of temperature in the mixed layer, the equation used is: dT = Q dt / ρ Cp dz, where Q is the net surface heat flux (e.g., Qs − Ql − Qh − Qe = shortwave, longwave, heat and evaporative components respectively), dt is time (one month), ρ is density, Cp is heat capacity, and dz is an average mixed layer depth (taken here as 15 m; e.g., *Levitus and Boyer*'s [1994] climatology suggests a range 10–30 m). *Enfield* [1986] used similar methods to obtain Q and dT estimates for the equatorial Pacific. All components of Q are obtained from the NCEP reanalysis model as departures from the mean with units W m^{-2}. *Fasullo and Webster* [1999] suggest that monthly net heat fluxes from the NCEP model are useful in determining the interannual variability of SST.

[29] In situ measurements of surface fluxes and upper ocean structure [*Majodina et al.*, 2002] reveal lifting of the thermocline in the 0°–10°S band from 50°–90°E. The uplift of cooler waters is attributable to cyclonic curl in
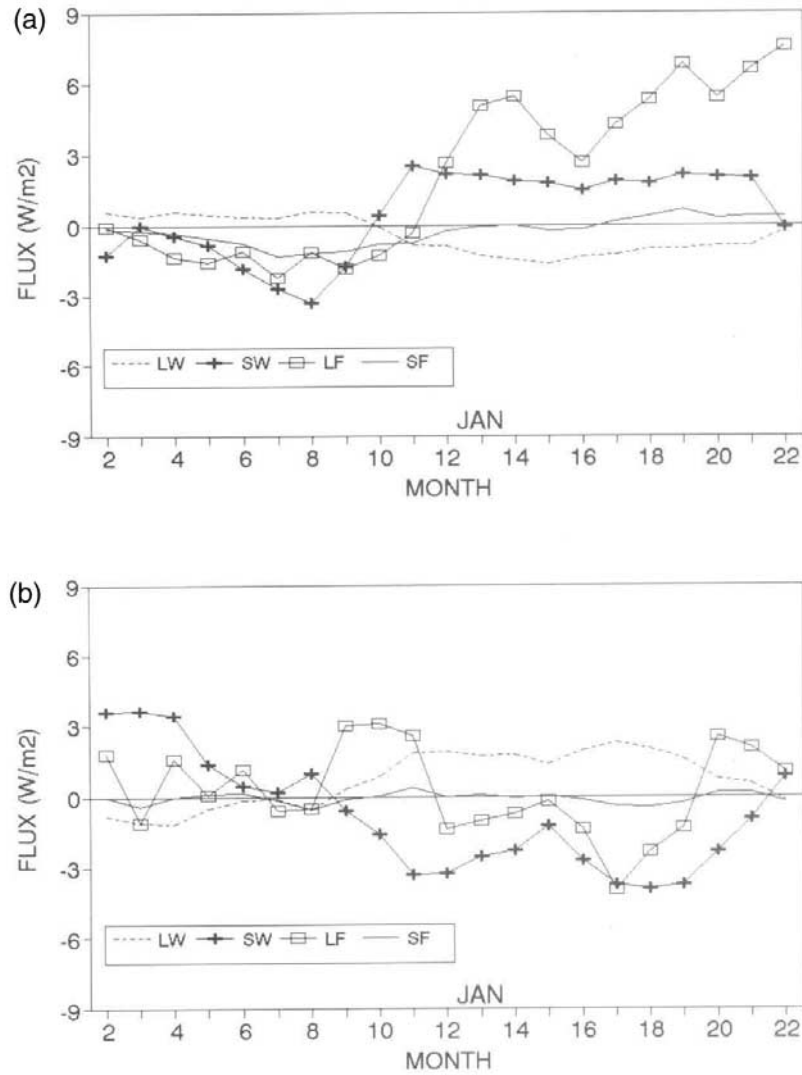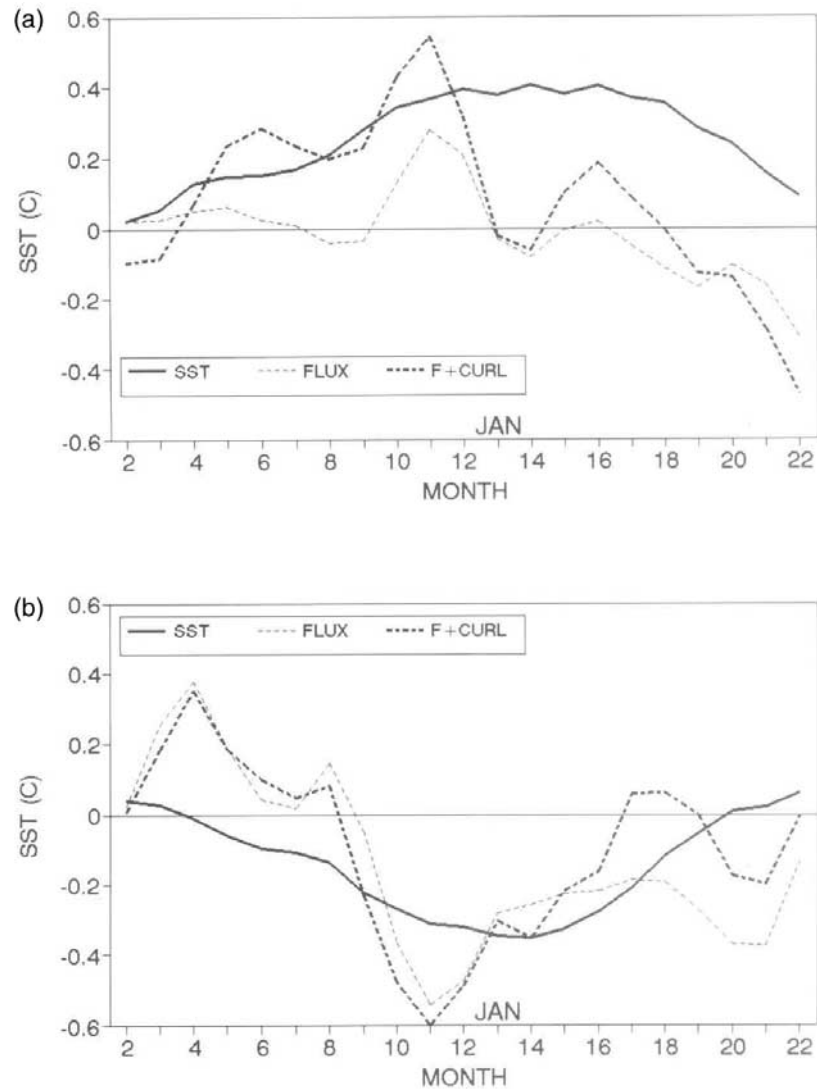
Figure 11. Composite (a) warm events (events 70, 73, 83, 87, 92, and 98) and (b) cool events (events 65, 72, 74, 76, 89, and 97) in the west-central Indian Ocean identifying surface flux components of the heat budget.

the surface wind field, which is sustained for much of the year south of the equator [*McCreary et al.*, 1993]. There are a number of assumptions involved in relating curl to dT via vertical entrainment. One is that the diabatic heating rate can be equated to the vertical advection at the mixed layer base, W*dT/dz, and a second is that all of the Ekman divergence responsible for the vertical velocity (W) is contained within the mixed layer. Typically, a lack of profile data imposes additional observational assumptions about the constancy, seasonality and geographic uniformity of an assumed upper ocean thermal profile. In view of these, a conservative approach is adopted. We determine the percentage departure from the mean curl based on monthly NCEP wind data and calculate vertical motion anomalies using $W = \tau_{curl}/\rho f$, from which we obtain dT = W (dT/dz) dt. The influence on mixed layer temperature is estimated using an average dT/dz of order 10^{-2} C m^{-1} from the *Levitus'* [1994] climatology (IRI/LDEO website). A scale analysis of the equation for vertical motion using typical values yields:

$\tau_{curl} = 10^{-7}$, $\rho = 10^{3}$, $F = 10^{-5}$, and $W = 10^{-5}$. An order of magnitude departure of τ_{curl} (1σ) can generate a monthly uplift of 10 m and a dT (monthly change of SST) of order 0.1°C. Because this approach relies on a climatological value for mixed layer stratification, departures may lead to errors in our estimate of entrainment influence. With west-central Indian Ocean SST near the convective threshold ~28°C, small changes in SST can result in significant changes in thermodynamic energy conversion (e.g., latent heating of the troposphere), so altering the surrounding climate.

[30] Warm events start with a near zero SST anomaly and rise gradually to a minor plateau in months 4–7 (April–July) of the onset year. During this time the wind field exhibits an increasing anticyclonic curl which deepens the oceanic thermocline south of the equator. Evaporative flux anomalies remain near zero early in the event. A steep increase of SST occurs in months 8–10 as the evaporative flux declines and the curl continues an anticyclonic trend.

Figure 12. Composite (a) warm events and (b) cool events in the west-central Indian Ocean illustrating observed (bold) and predicted (thin dashed lines) SST anomalies.

The estimated shortwave radiation exhibits a negative tendency and plays a minor role until months 11–13 (Nov to Jan+1) when positive values occur. The anticyclonic curl and evaporative flux anomalies weaken at the mature stage of the warm event. The warm SST anomaly reaches a value of +0.4 C from months 11 to 17 (Oct to May+1), a lengthy spell coinciding with the NE monsoon. Anticyclonic wind curl provides a warming influence in months 16–18 (April to June+1) and the estimated shortwave radiation increases thereafter, inhibiting dissipation of the warm event, despite a positive heat flux anomaly. Finally, SST anomalies remain positive while the flux and curl influence contribute to cooling after January. The predicted SST based on both fluxes and curl are consistent with the composite observed values from months 5 to 12, and suggest that ocean-atmosphere interactions can account for the build-up of the warm event rather well. In the decay stage, significant differences between observed and predicted values may be attributable to warm advection by ocean currents and thermal inertia.

[31] The cool event is somewhat different in character, suggesting a degree of nonlinear behavior for ocean-atmosphere coupling. SST declines to a minimum more symmetrically in months 11–15 (Nov to Mar+1). The onset phase displays a weak plateau for SST in the months 6–8, following a sharp increase in evaporative flux in month 5 (May). The curl influence is minimal through the onset and mature stages of the cool event. Composite fluxes do not generate 'sufficient' cooling in the initial stages of the event. However, by months 9–11 evaporation strengthens considerably. The estimated shortwave radiation exhibits a sharp decline from month 8 to 11 (Nov) and remains below normal through much of the cold event (to month 22). SST anomalies begin to rise rapidly in months 16–20 (Apr to Aug+1) as the southwest monsoon prevails. The monsoon circulation yields an anticyclonic curl influence from months 17–19 (May to July+1) which rapidly dissipates the cool event. In general, SSTs are overpredicted by the composite net flux plus curl components during the OND season.

Table 2. Pairwise Correlations (r^2%)

Rainfall Area	Monsoon Indices[a]
West Africa	cAu_2 (30),[b] cAu (26),[b] swIsst (26)[b]
West Afr-6	nwIp (37),[b] cAu_2 (35),[b] eIp (22)[b]
South. Afr	swIsst (16),[b] wIv (12),[b] swAsst (8)
South. Afr-6	eIu (13),[b] wIv (12),[b] cIΨ (6)
East Africav	eIu (34),[b] cAu(8), cIsst (7)
East Afr-6	eIu (13),[b] cAu (10)[b]

[a] First lower case = area; second upper case = ocean; third lower case = parameter; −6 = lead time; and top three indices are retained.
[b] Values significant at 95%.

[32] Contrasts between the composite events can be found in the slow decay of the warm event and its greater amplitude. The estimated shortwave radiation follows the SST anomaly, and supports the wind influence (e.g., flux and curl). This is unexpected: an increase of SST should result in locally increased cloud and reduced radiative energy, hence negative feedback. Here the evaporative flux, wind curl and solar radiation are constructively engaged. The τ_{curl} leads the warm events and predicted – observed residuals are small from months 6–12. However, neither the surface fluxes nor curl (vertical motion) explain the onset of cool events, so it is presumed that cooling is initiated through oceanic advection associated with basin-scale wave propagation, as outlined by Huang and Kinter (submitted manuscript, 2001). The influences are quite seasonal: in both cases the surface heat fluxes are strong in the OND season, while the τ_{curl} contributes in the JAS season preceding the warm event, a useful result for predictive purposes.

3.3. Associations Between Monsoon Indices and Continental Rainfall 1958–1988

[33] In this section we apply the monsoon indices to interannual fluctuations of continental rainfall over a 31 year period. Our aim is to determine how well the ENSO-monsoon interactions explain the rainfall fluctuations at concurrent and 6 month lead time. By separately considering the three highest correlated predictors for each rainfall series, a number of interesting features can be noted (Table 2). Correlation values are higher for a wider selection of indices in the case of West African rainfall owing to its larger persistence (serial correlation). The central Atlantic upper and lower zonal winds (cAu_2, cAu) are influential at concurrent times, while pressure over the Arabian Sea (nwIp) is closely associated with West African rainfall at 6 month lead time. For southern African rainfall, meridional flow over the west Indian Ocean (wIv) and SST in the SW Indian Ocean are important, while zonal winds over the east Indian Ocean are related at 6 month lead. Zonal winds in the east Indian Ocean (eIu) are quite influential to East African rainfall, while zonal winds over the central Atlantic are also associated.

[34] The regression models are formulated using a forward stepwise regression technique up to a maximum of three predictors as outlined by Jury et al. [1999]. The resultant predictors are screened for colinearity against a r^2 threshold of 20%. A 95% significant hindcast fit is achieved when the multiple r^2 value exceeds 30% for West Africa and 27% for southern and east Africa, including the artificial skill imposed by a candidate pool of 13 predictors over a training period of 31 years. With the time series normalized,

the regression coefficients may be assessed to determine the degree of influence of the various monsoon indices on African climate. The multivariate models (Table 3) often differ from pairwise assessments (Table 2). Within our 31 year record, decadal signals and model stability may not be resolved.

[35] From the algorithms listed in Table 3, the following interpretations can be made. West African rainfall is associated with surface zonal winds in the central Atlantic. Significantly, all African rainfall areas use this predictor with positive sign, e.g., westerly flow → wet conditions. At zero lag the north-south SST gradient in the Atlantic Ocean is an important determinant, the south having greater influence. Cooler conditions in the southeast Atlantic contribute to a northward migration of the ITCZ over the Sahel as expected [Servain, 1991]. At 6 month lead surface air pressure in the north Indian Ocean is important and may relate to precursor conditions for easterly wave trains. The model fit is significant (>40%) at both simultaneous and 6 month lead for West Africa.

[36] The zero lag model for southern Africa is closely related to the meridional gradient of SST over the Indian Ocean. When the tropics (subtropics) are cooler (warmer) than normal, greater rainfall is produced by a southward migration of the ITCZ and a weakening of upper westerly winds. The 6 month lead model for southern Africa uses the SW Indian SST together with zonal winds in the east Indian Ocean and the stream function (curl) over the central Indian Ocean. A cyclonic rotation induces an uplift of cooler subsurface water, favoring increased rainfall over southern Africa. The model only explains 26% of variance at 6 month lead.

[37] The east African rainfall model uses zonal winds over the east Indian Ocean, but with opposite sign to the southern region. Easterly flow in the east Indian Ocean favors wet conditions concurrently and at 6 month lead. Westerly surface winds over the central Atlantic are associated with increased rainfall over east Africa both concurrently and in advance. At 6 month lead a warmer SW Indian Ocean (+swIst) creates a precursor environment for increased rainfall, with the same sign as for southern Africa.

[38] Multiple regression models using monsoon indices are able to replicate 40–44% of simultaneous rainfall variance respectively for southern and east Africa. These values are statistically significant, and are largely dependent on the use of atmospheric predictors at long lead times. This may be explained in terms of our earlier analysis, wherein winds lead the tropical oceans through various dynamical processes, from equatorial upwelling (Atlantic) to conspiring fluxes and curl (Indian). This being the case, we may conclude that atmospheric signals in ocean monsoon

Table 3. Multivariate Models[a]

Rainfall Area	Linear Regression Algorithm	Adjusted r^2 Fit%
West Africa	+0.71(cAu) −0.44(seAsst) +0.19(nAsst)	44
West Afr-6	−0.33(nwIp) −0.25(seAsst) +0.24(cAu)	43
South. Afr	+0.63(swIsst) −0.43(cIsst) +0.22(cAu)	40
South. Afr-6	+0.27(eIu) +0.26(swIsst) +0.22(cIΨ)	26
East Africa	−0.68(eIu) +0.36(cAu)	44
East Afr-6	+0.51(cAu) −0.36(eIu) +0.30(swIsst)	32

[a] First lower case = area; second upper case = ocean; third lower case = parameter; −6 refers to lead time.

Table 4. Seasonal Relationships for Key Predictors

Rainfall Area	Predict time	Pairwise Correlation (r^2%)
West Afr-6	January:	nwIp (41),[a] cAu (27),[a] seAsst (10) +a
	July:	nwIp (46),[a] cAu (12), +a seAsst (8)
South. Afr-6	July:	eIu (8), cIΨ (7), swIsst (3)
	January:	swIsst (10),[a] cIΨ (3), eIu (2)
East Afr-6	April:	eIu (37),[a] cAu (14) +a
	October:	eIu (15),[a] cAu (11)[a]

[a] Values significant at 95%.

regions exhibit sufficient memory to qualify as candidate predictors of terrestrial climate.

[39] To investigate how the monsoon indices influence African rainfall at different times of the year, we disaggregate the series into 3 month seasons and assess associations with the leading predictor at 6 month lead time (Table 4). For West African rainfall the more useful DJF to JJA association operates for the nwIp and cAu predictors, while declining values are found for the others. In the case of Southern Africa, the more 'useful' JJA to DJF association holds for the eIu and cIΨ variables, but the swIsst variable shows a decline. For the bimodal East African rainfall, the cAu and eIu predictors associate more closely in April than October, suggesting that the SON rains are more predictable than the MAM rains, as expected.

4. Discussion and Conclusions

[40] African climates are dominated by the monsoon circulations that extend across the east Atlantic and west Indian Oceans. In the May to September period the Indian southwest monsoon draws moisture away from east Africa, while the tropical Atlantic monsoon feeds easterly waves north of the Guinea coast [*Eltahir and Gong*, 1996; *Druyan and Hall*, 1996]. From November to March, the NE monsoon sweeps across the west Indian Ocean delivering moisture, first to east Africa and later to southern Africa and the Mascarene Islands. The center of convective activity over the Congo basin shifts with solar angle and the seasonal monsoons. Axes of upward motion from the continental heat source extend southeastward during the austral summer to the Indian ITCZ, and westward to the Atlantic ITCZ in boreal summer. Over the central Indian Ocean the westerly monsoon flow is deep and upper easterlies are weak. Over the tropical Atlantic the westerlies are shallow and upper easterly flow is more strongly developed [*Hastenrath*, 2001].

[41] We have examined the way the monsoon circulations depart from normal and affect rainfall and hurricane development, using wavelet-based time series methods and multiple regression analysis. For the Indian Ocean, where prior studies have not explained the relationships between monsoon winds and SST (as in the Atlantic) we have analyzed the relationship of SST tendency with surface fluxes and entrainment for composites of warm events and cool events.

[42] The extent and intensity of monsoon-driven convection is dependent on the interaction of local and remote ocean-atmosphere coupling processes. Our research has shed light on this subject by examining the nature and stability of ENSO transmission through monsoon indices in key areas around Africa. One of the strongest relationships is that upper zonal winds in the Atlantic often lead Niño3

SST, particularly in the 1980s (Figure 5). This suggests the global direct circulation reacts quickly to the initial shift of convection anomalies from the western Pacific, compared with the slower nature of eastward ENSO propagation in the ocean. This direct circulation displays a shift in the 1970s, with maximum amplitude over west and southern Africa producing anomalous vertical motion that is consistent with the observed rainfall anomalies. *Richard et al.* [2000] have found a similar shift in the relationship between southern African rainfall and ENSO. Other factors involving gradients of Atlantic SST and consequent ITCZ migration may be of similar importance to the large scale forcing fields. In east Africa, rainfall appears to vary with anomalies of low-level winds over the monsoon region.

[43] Another of the monsoon associations seen in the wavelet analysis is an ENSO-related zonal see-saw variation in equatorial SST between the Indian and Atlantic Oceans. SST changes in the east Atlantic are antiphase to the equatorial Pacific and west-central Indian Oceans, (Figure 9). This is reminiscent of an Atlantic-Pacific SST see-saw found to be important for Caribbean and Central American rainfall [*Enfield and Alfaro*, 1999; *Giannini et al.*, 2000]. However, our multiple regression analysis did not select these inter-ocean SST swings as a predictor of African rainfall.

[44] Our understanding of ENSO-monsoon interactions around Africa has been applied to continental rainfall through development of multiple regression models. Regional rainfall indices were prepared using rotated principal component analysis for three coherent areas: Northwest (Sahel-Guinea), Southern (Kalahari-Zambezi), and East (Kenya-Tanzania). The statistical models for the three rainfall series make use of seven overlapping monsoon indices during the 1958–1988 period (Figure 3). For each region about 40% of the variance is explained by three key monsoon indices, which vary from one region to another. In certain cases the regression coefficient takes an opposing sign from one region to another.

[45] The variables most associated with the interannual variability of West African rainfall are the zonal Walker circulation over the central equatorial Atlantic and the SSTs in the tropical North Atlantic and southeast tropical Atlantic. The Walker cell is accelerated in association with El Niño in the Pacific, with increased westerlies aloft, high-level convergence and midtropospheric subsidence over West Africa, and less rainfall, as observed [*Ward et al.*, 1999, Figures 2a, 5, and 6]. The Walker acceleration is also consistent with increased surface easterlies in the Gulf of Guinea region, southerly anomalies across the ITCZ and weakened NE trades over the tropical North Atlantic. This altered surface wind pattern is consistent with the boreal winter-spring warming of the tropical North Atlantic following the early boreal winter peak in Niño3 anomalies [*Enfield and Mayer*, 1997].

[46] The Sahelian dryness associated with El Niño [*Ward et al.*, 1999] is consistent with the Walker cell anomaly but not with the tropical North Atlantic warming. The non-ENSO CCA (canonical correlation analysis) mode of *Ward et al.* [1999] shows the opposite relation of Sahel rainfall to tropical Atlantic SST from their ENSO mode, that is, a warm tropical North Atlantic (cool tropical South Atlantic) is associated with increased Sahel rainfall. This is the conventional expectation for the Sahel-SST relationship.

This dichotomy, and the fact that the Walker anomalies tend to precede the Niño3 peak, are indications that the ENSO-related rainfall anomaly is being forced tropospherically from the early El Niño convection anomaly near the date-line, and not in response to local SST changes. Conversely, one can speculate that non-ENSO Sahel rainfall anomalies respond to tropical Atlantic SST, in the expected manner.

[47] The accelerated Walker cell (above) coincides with increased vertical shear, both over the equator and extending northward to the 5°–15°N region. The increased tropospheric shear and greater tropical North Atlantic SSTs are consistent with subsequent reduced hurricane activity downstream in the main development region west of Africa (Figure 8). At 6 month lead the surface pressure in the north Indian Ocean is lower prior to increased rainfall over West Africa. This area is upstream and in the same latitudinal belt as the tropical easterly jet which overlies Sahelian wave trains during boreal summer. When upper easterlies are strong, easterly waves are more active within the African ITCZ [*Druyan and Hall*, 1996].

[48] Again, as with the Sahel rainfall, the well known tendency for tropical North Atlantic SST to warm during the boreal spring following the Pacific El Niño peak is physically inconsistent with the observed decrease in hurricane activity shown here and by Gray and others. This can be understood in two ways. First, it has been demonstrated by hurricane researchers that the shear effect is more important than the SST in determining tropical storm development, or lack thereof [*Goldenberg et al.*, 2001; *Zehr*, 1992]. More importantly, the shear effect, being connected directly via the troposphere to the El Niño convection near the dateline most frequently affects the hurricane season prior to the Niño3 peak as opposed to the season after the Niño3 peak when El Niño has typically ended [*Landsea et al.*, 1999; C. W. Landsea, personal communication, 2000]. Hence, the shear influence on hurricanes most frequently does not conflict with the SST influence, and in cases where it does, the shear effect is likely to dominate.

[49] For southern African rainfall, SST differences between the southwest and central Indian Ocean and the rotational component of monsoon flow in the central Indian Ocean (which controls Ekman divergence and ocean entrainment) play significant roles. For east African rainfall, the surface zonal wind in the east equatorial Indian Ocean is a key determinant. Westerly (easterly) winds in the east Indian Ocean favor rainfall in southern (east) Africa, and serve to indicate the strength of the zonal direct circulation and the east-west SST gradient. The implication is that East Africa shares a maritime rainfall regime with the west Indian Ocean, while convection over southern Africa is inversely related.

[50] The composite ocean thermal analysis performed for extreme warm and cool events in the west-central Indian Ocean describes their initiation and maintenance. Composite warmings begin and are maintained through the alternate or simultaneous effects of reduced evaporation and reduced entrainment, while increased radiative fluxes also contribute. The OND season is when the fluxes most actively modify SST, and also when the ocean and atmosphere are most strongly coupled (e.g., cloud depth adjusts to SST). Considering the net heat fluxes and vertical motion induced by the wind curl, the predicted amplitude and phase of SST warming and cooling conforms well with observed values. Discrepancies occur in the decay phase of the warm event, and in the onset phase of the cool event. The unexplained residuals suggest that advective processes may play an important role at those times.

[51] A brief study of the seasonality of target-predictor relationships was made. In general, statistical associations are distributed across the year and are not particularly phase-locked. For the predictors zonal wind (eIu, cAu) and pressure (nwIp), the association is stronger leading into the rainy season. However, the SST predictors (seAsst, swIsst) relate more strongly leading into the dry season. This finding provides support for the use of monsoon indices in predictive models. Recognizing that our knowledge of ocean-atmosphere coupling around Africa is limited, it is suggested that greater in situ measurements be gathered as part of GOOS and Climate Variability and Predictability program (CLIVAR) activities.

[52] Decadal variability can also be seen in some of the monsoon indices but is not well resolved by the 1958–1988 data sets. One example is the relationship between hurricane development, North Atlantic SST and tropospheric wind shear (Figure 7), which is consistent with the findings of others. Another example is an increase in westerly flow aloft over the equatorial Atlantic, which corresponds well to a shift in Pacific SSTs and the global direct circulation in the late 1970s [*Mestas-Nuñez and Enfield*, 2001]. The greater westerly flow aloft feeds an increased upper tropospheric convergence over West Africa, suggesting that reduced convection (increased subsidence) over that region is a factor in the drier Sahel conditions observed in recent decades.

Appendix A: Cross-Wavelet Spectrum and Estimation of the Instantaneous Phase Difference and Time Lag Between Two Time Series

[53] The continuous wavelet transform (CWT) of a signal $x(t)$ with wavelet ψ is defined as

$$W_x(b,a) = \frac{1}{a} \int_{-\infty}^{\infty} x(t)\psi^*\left(\frac{t-b}{a}\right)dt, \qquad (A1)$$

where a is the dilatation parameter, b is the time translation parameter and * denotes the complex conjugate. Here, we use the complex Morlet wavelet:

$$\psi(t) = \pi^{-1/4}\exp\left(-t^2/2\right)\exp(i\omega_0 t), \qquad (A2)$$

with $i = \sqrt{-1}$ and $\omega_0 = \sqrt{2/\ln 2} \cong 5.34$. With this wavelet, the transform coefficient $W_x(b,a)$ may be expressed in terms of real and imaginary parts, modulus and phase, and the relation between the dilation parameter a and frequency f is $f(a) = \omega(a)/2\pi = 0.874/a$.

[54] The cross-wavelet spectrum of two series $x(t)$ and $y(t)$ is defined as

$$W_{xy}(b,a) = W_x(b,a)W_y^*(b,a), \qquad (A3)$$

where $W_x(b,a)$ and $W_y(b,a)$ are the CWT of $x(t)$ and $y(t)$ respectively and where * denotes the complex conjugate.

The cross-wavelet coefficient $W_{xy}(b, a)$ is a complex number and may be expressed in terms of real and imaginary parts, modulus and phase difference. Recall that if and $z_1 = c_1 \exp(i\theta_1)$ and $z_2 = c_2 \exp(i\theta_2)$ are two complex numbers with phases θ_1 and θ_2, then $z_1 z_2^* = c_1 c_2 \exp[i(\theta_1 - \theta_2)]$ is a complex number with phase: $\Delta\theta = \theta_1 - \theta_2$.

[55] Consequently, the cross-wavelet spectrum provides an estimation of the local phase difference $\Delta\phi(b, a)$ between the two series for each point of the (b, a) time-frequency space. This local phase difference is independent of the amplitude of the series. These characteristics allow us to estimate the instantaneous phase difference between the two series $x(t)$ and $y(t)$. Keeping in mind that b corresponds to the time t, this phase difference is defined as

$$\Delta\Phi(b) = \tan^{-1} \frac{\int_{a1}^{a2} \text{Im}[W_{xy}(b, a)]da}{\int_{a1}^{a2} \text{Re}[W_{xy}(b, a)]da}, \qquad (A4)$$

where $\text{Re}[W_{xy}(b, a)]$ and $\text{Im}[W_{xy}(b, a)]$ are the real and imaginary parts of $W_{xy}(b, a)$ and where $a_1 < a_2$ are the lower and upper limits of the dilatation parameter. The instantaneous time lag between $x(t)$ and (t) is then obtained from the relation

$$T(b) = \frac{\Delta\Phi(b)}{2\pi F(b)}, \qquad (A5)$$

where $F(b)$ is the instantaneous frequency. We define this frequency as the first normalized moment in frequency of $W_{xy}(b, a)$:

$$F(b) = \frac{\int_{a1}^{a2} f(a)|W_{xy}(b, a)|da}{\int_{a1}^{a2} |W_{xy}(b, a)|da}, \qquad (A6)$$

where $f(a)$ is the frequency corresponding to the dilation parameter a and where $|W_{xy}(b, a)|$ is the modulus of $W_{xy}(b, a)$.

References

Bigot, S., P. Camberlin, V. Moron, and P. Raucou, Modes of rainfall variability in tropical Africa and their stability through time, paper presented at 21st Conference on Hurricane and Tropical Meteorology, Am. Meteorol. Soc., Miami, 1995.

Cadet, D. L., The Southern Oscillation over the Indian Ocean, J. Clim., 5, 189–212, 1985.

Camberlin, P., Drought and seasonal rainfall variance in the horn of Africa, paper presented at 1st International Conference of the African Meteorolocal Soceity, Nairobi, Kenya, 1995.

Chambers, D. P., B. D. Tapley, and R. H. Stewart, Anomalous warming of the Indian Ocean coincident with El Niño, J. Geophys. Res., 104, 3035–3047, 1999.

Delprat, N., B. Escudé, P. Guillemain, R. Kronland-Martinet, P. Tchamitchian, and B. Torrésani, Asymptotic wavelet and Gabor analysis: Extraction of instantaneous frequencies, IEEE Trans. Info. Theory, 38, 644–664, 1992.

Druyan, L., and T. Hall, The sensitivity of African wave disturbances to remote forcing, J. Appl. Meteorol., 35, 1100–1110, 1996.

Eltahir, E. A. B., and C. Gong, Dynamics of wet and dry years in West Africa, J. Clim., 9, 1030–1042, 1996.

Enfield, D. B., Zonal and seasonal variations of the near-surface heat balance of the equatorial Pacific Ocean, J. Phys. Oceanogr., 16, 1038–1054, 1986.

Enfield, D. B., and E. J. Alfaro, The dependence of Caribbean rainfall on the interaction of the tropical Atlantic and Pacific Oceans, J. Clim., 11, 2093–2103, 1999.

Enfield, D. B., and D. A. Mayer, Tropical Atlantic sea surface temperature variability at its relation to El Niño-Southern Oscillation, J. Geophys. Res., 102, 929–945, 1997.

Enfield, D. B., A. M. Mestas-Nunez, D. A. Mayer, and L. Cid-Serran, How ubiquitous is the dipole relationship in the tropical Atlantic sea surface temperatures?, J. Geophys. Res., 104, 7841–7848, 1999.

Fasullo, J., and P. J. Webster, Warm pool SST variability in relation to the surface energy balance, J. Clim., 12, 1292–1305, 1999.

Giannini, A., Y. Kushnir, and M. A. Cane, Interannual variability of Caribbean rainfall, ENSO, and the Atlantic Ocean, J. Clim., 13, 297–311, 2000.

Gill, A. E., Some simple solutions for heat-induced tropical circulation, Q. J. R. Meteorol. Soc., 106, 447–462, 1980.

Goddard, L., and N. L. Graham, Importance of the Indian Ocean for simulating rainfall anomalies over eastern and southern Africa, J. Geophys. Res., 104, 19,099–19,116, 1999.

Goldenberg, S. B., and L. J. Shapiro, Physical mechanisms for the association of El Niño and West African rainfall with Atlantic major hurricane activity, J. Clim., 9, 1169–1187, 1996.

Goldenberg, S. B., C. W. Landsea, and W. M. Gray, The recent increase in Atlantic hurricane activity: Causes and implications, Science, 293, 474–479, 2001.

Gray, W., Atlantic hurricane frequency, part 1, El Niño and 30 mb quasi-biennial oscillations influences, Mon. Weather Rev., 112, 1649–1668, 1984.

Harrison, M., A synoptic climatology of South African rainfall variations, Ph.D. thesis, 341 pp., Univ. Witwatersrand, Johannesburg, South Africa, 1986.

Hastenrath, S., Zonal circulations over the equatorial Indian Ocean, J. Clim., 21, 2746–2756, 2000.

Hastenrath, S., In search of zonal circulations in the equatorial Atlantic sector from the NCEP-NCAR reanalysis, Int. J. Climatol., 21, 37–48, 2001.

Hastenrath, S., A. Nicklis, and L. Greischar, Atmospheric-hydrospheric mechanisms of climate anomalies in the western equatorial Indian Ocean, J. Geophys. Res., 98, 20,219–20,235, 1993.

Hirst, A. C., and S. Hastenrath, Atmosphere-ocean mechanisms of climate anomalies in the Angola-Tropical Atlantic sector, J. Phys. Oceanogr., 13, 1146–1157, 1983.

Janicot, S., A. Harzallah, B. Fontaine, and V. Moron, West African monsoon dynamics and eastern equatorial Atlantic and Pacific SST anomalies (1970–88), J. Clim., 11, 1874–1882, 1998.

Janowiak, J. E., An investigation of interannual rainfall variability in Africa, J. Clim., 1, 240–255, 1988.

Jury, M. R., and B. Pathack, Composite climatic patterns associated with extreme modes of summer rainfall over southern Africa: 1975–1984, Theor. Appl. Climatol., 47, 137–145, 1993.

Jury, M. R., C. McQueen, and K. M. Levey, SOI and QBO signals in the African region, Theor. Appl. Climatol., 50, 103–111, 1994.

Jury, M. R., H. M. Mulenga, and S. J. Mason, Exploratory long-range models to estimate summer climate variability over southern Africa, J. Clim., 12, 1892–1899, 1999.

Kalnay, E., et al., The NCEP/NCAR reanalysis 40-year project, Bull. Am. Meteorol. Soc., 77, 437–471, 1996.

Landsea, C. W., R. A. Pielke, and J. A. Knaff, Atlantic basin hurricanes: Indices of climatic change, Clim. Change, 42, 89–129, 1999.

Latif, M., and T. P. Barnett, Interactions of the tropical oceans, J. Clim., 8, 952–968, 1995.

Lau, K. M., and H. Y. Weng, Climate signal detection using wavelet transform: How to make a time series sing, Bull. Am. Meteorol. Soc., 76, 2391–2402, 1995.

Levitus, S., and T. P. Boyer, World Ocean Atlas 1994, vol. 4, Temperature, NOAA Atlas NESDIS, vol. 4, 129 pp., Natl. Oceanic and Atmos. Admin., Silver Spring, Md., 1994.

Long, M., D. Entekhabi, and S. E. Nicholson, Interannual variability in rainfall, water vapour flux and vertical motion over West Africa, in Water

Resources Variability in Africa, edited by E. Servat et al., IAHS Publ., *252*, 27–33, 1998.

Majodina, M., M. R. Jury, and M. Rouault, Ocean-atmosphere structure in the tropical Indian Ocean during a ship cruise 1995/96, *Global Ocean Atmos. Syst.*, in press, 2002.

Mallat, S., *A Wavelet Tour of Signal Processing*, Academic, San Diego, Calif., 1998.

McCreary, J. P., P. K. Kundu, and R. Molinari, A numerical investigation of the dynamics and thermodynamics and mixed layer processes in the Indian Ocean, *Prog. Oceanogr.*, *31*, 181–244, 1993.

Mestas-Nuñez, A. M., and D. B. Enfield, Eastern equatorial Pacific SST variability: ENSO and non-ENSO components and their climatic associations, *J. Clim.*, *14*, 391–402, 2001.

Meyers, S. D., B. G. Kelley, and J. J. O'Brien, An introduction to wavelet analysis in oceanography and meteorology: With application to the dispersion of Yanai waves, *Mon. Weather Rev.*, *121*, 2858–2866, 1993.

Mpeta, E. J., and M. Jury, Intra-seasonal convective structure and evolution over tropical east Africa, *Clim. Res.*, *17*, 83–92, 2001.

Mutai, C. C., M. N. Ward, and A. W. Colman, Towards the prediction of the east Africa short rains based on sea-surface temperature-Atmosphere coupling, *Int. J. Climatol.*, *18*, 975–998, 1998.

Nicholson, S. E., The spatial coherence of African rainfall anomalies: Interhemispheric teleconnections, *J. Clim. Appl. Meteorol.*, *25*, 1365–1381, 1986.

Nicholson, S. E., An analysis of the ENSO signal in the tropical Atlantic and western Indian Oceans, *Int. J. Climatol.*, *17*, 345–375, 1997.

Nicholson, S. E., and B. S. Nyenzi, Temporal and spatial variability in the tropical Atlantic and Indian Oceans, *Meteorol. Atmos. Phys.*, *41*, 1–17, 1990.

Peixoto, J. P., Atmospheric energetics and the water cycle, in *Energy and Water Cycles in the Climate System, Nato ASI Ser.*, vol. 15, chap. 1, pp. 1–421, edited by E. Raschke and D. Jacob, Springer-Verlag, New York, 1993.

Quenouille, M. H., *Associated Measurements*, 242 pp., Butterworths, London, 1952.

Reason, C. J., and H. Mulenga, Relationships between South African rainfall and SST anomalies in the southwest Indian Ocean, *Int. J. Climatol.*, *19*, 1651–1673, 1999.

Reason, C. J. C., R. J. Allan, J. A. Lindesay, and T. J. Ansell, ENSO and climatic signals across the Indian Ocean basin in the global context, part 1, Interannual composite patterns, *Int. J. Climatol.*, *20*, 1285–1327, 2000.

Reynolds, R. W., and M. Smith, Improved global sea surface temperature analyses using optimum interpolation, *J. Clim.*, *7*, 929–948, 1994.

Richard, Y., Variability of rainfall in West Africa, *Meteorologie*, *8*, 11–22, 1994.

Richard, Y., S. Trzaska, P. Roucon, and M. Rouault, Modification of the southern African rainfall variability/ENSO relationship since the late 1960s, *Clim. Dyn*, *16*, 883–895, 2000.

Rocha, A. M. C., and I. Simmonds, Interannual variability of south-east African summer rainfall, part I, Relationships with air-sea interaction processes, *Int. J. Climatol.*, *17*, 235–265, 1997.

Rwelamira, J. K., and T. E. Kleynhans, SADC agricultural potential assessment-Country profiles, DBSA Rep. 124, Dev. Bank of S. Afr., South Africa, 1996.

Saji, N. H., B. N. Goswami, P. N. Vinayachandran, and T. Yamagata, A dipole mode in the tropical Indian Ocean, *Nature*, *401*, 360–363, 2001.

Schiller, A., How well does a coarse-resolution circulation model simulate observed interannual variability in the upper Indian Ocean?, *Geophys. Res. Lett.*, *26*, 1485–1488, 1999.

Schiller, A., J. S. Godfrey, P. C. McIntosh, G. Meyers, and R. Fiedler, Interannual dynamics and thermodynamics of the Indo-Pacific Oceans, *J. Phys. Oceanogr.*, *30*, 987–1012, 2000.

Servain, J., Simple climatic indices for the tropical Atlantic Ocean and some applications, *J. Geophys. Res.*, *96*, 15,137–15,146, 1991.

Servain, J., I. Wainer, A. Dessier, and J. P. McCreary, Modes of climatic variability in the tropical Atlantic, 1998, in *Water Resources Variability in Africa*, edited by E. Servat et al., IAHS Publ., *252*, 45–51, 1998.

Torrence, C., and G. P. Compo, A practical guide to wavelet analysis, *Bull. Am. Meteorol. Soc.*, *79*, 61–78, 1997.

Ward, M. N., P. J. Lamb, D. H. Portis, M. El Hamly, and R. Sebarri, Climate variability in northern Africa: Understanding droughts in the Sahel and the Maghreb, in *Beyond El Niño—Decadal Variability in the Climate System*, edited by A. Navarra, pp. 119–140, Springer-Verlag, New York, 1999.

Webster, P. J., A. M. Moore, J. P. Loschnigg, and R. R. Leben, Coupled ocean-atmosphere dynamics in the Indian Ocean during 1997–1998, *Nature*, *401*, 356–360, 1999.

White, W. B., and D. R. Cayan, A global El Niño-Southern Oscillation wave in surface temperature and pressure and its interdecadal modulation from 1900 to 1997, *J. Geophys. Res.*, *105*, 11223–11242, 2000.

Woodberry, K. E., and M. E. Luther, The wind-driven seasonal circulation in the southern tropical Indian Ocean, *J. Geophys. Res.*, *94*, 17,985–18,002, 1989.

Zebiak, S. E., Air-sea interaction in the equatorial Atlantic region, *J. Clim.*, *8*, 1567–1586, 1993.

Zehr, R. M., Tropical cylogenesis in the western North Pacific, NOAA Atlas NESDIS, vol. 61, 181 pp., Natl. Oceanic and Atmos. Admin., Silver Spring, Md., 1992.

─────────────

D. B. Enfield, Atlantic Oceanography and Meteorology Lab, National Oceanic and Atmospheric Administration, Miami, FL 33149, USA. (David.Enfield@noaa.gov)

M. R. Jury, Geography Department, University of Zululand, 3886 Zululand, South Africa.

J.-L. Mélice, Centre IRD de Bretagne, B. P. 70, F-29280 Plouzané, France.